Quantum State Characterization: Classical Shadows vs. Quantum State Tomography

Andre Figueroa

December 1, 2025

Abstract

We compare two quantum state reconstruction techniques—Pauli-based quantum state tomography (QST) and the classical shadows protocol—using a single transmon qubit in the QLab/OPX hardware environment. Both methods reconstruct the Bloch vector, density matrix, and fidelity of a prepared $|+\rangle$ state. We analyze measurement efficiency and reconstruction accuracy using experimental data from the same device. In our latest runs, classical shadows achieve essentially the same fidelity as QST while using fewer structured measurement settings. The wall-clock runtime is slightly shorter for classical shadows but remains dominated by control overhead, illustrating that the main advantage of shadows is measurement efficiency and scalability rather than raw speed in the single-qubit regime.

1 Introduction

Quantum state characterization is central to quantum computing experiments. The standard approach, Pauli-based quantum state tomography (QST), reconstructs the density matrix ρ by measuring a complete set of Pauli observables. For a single qubit, this requires measuring in three bases (X, Y, Z), and for n qubits, requires 3^n measurement settings and $O(4^n)$ parameters, making QST exponentially expensive.

Classical shadows, introduced by Huang, Kueng, and Preskill [1], provide a scalable alternative. Rather than measuring deterministically in each Pauli basis, the experiment randomly samples a basis per shot. The resulting "shadow" allows efficient prediction of many observables from the same dataset, with sample complexity that scales with the number of observables rather than the full state dimension.

This project benchmarks QST and classical shadows on a superconducting transmon qubit prepared in the state $|+\rangle$. We compare Bloch vectors, density matrices, fidelities, runtime, and shot efficiency. Our goal is to characterize the practical performance difference between QST and classical shadows on real hardware.

2 Methods

2.1 Hardware and Calibration Prerequisites

Experiments were run on a single transmon qubit (device label q4) using the Quantum Machines OPX+ controller. Required calibrations (performed beforehand) include:

- resonator spectroscopy,
- Rabi calibration of X_{90} and Y_{90} pulses,
- readout optimization (IQ discrimination mapping),
- Ramsey measurements for precise qubit frequency.

The target state $|+\rangle$ is prepared using a calibrated Y_{90} pulse:

$$|+\rangle = \frac{1}{\sqrt{2}}(|0\rangle + |1\rangle).$$

Active reset is used throughout the experiment to minimize dead time between shots.

2.2 Classical Shadow Protocol

For each shot, we perform:

1. active reset,
2. state preparation via Y_{90},
3. random choice of Pauli basis:

$$P \in \{X, Y, Z\} \text{ with equal probability,}$$

4. basis rotation (e.g., Y_{90} for X measurement, $-X_{90}$ for Y measurement, identity for Z),
5. computational-basis measurement.

A total of 1000 shots were taken. The distribution of sampled bases was:

$$X = 326, \quad Y = 349, \quad Z = 325,$$

which is close to uniform.

For each measurement, the outcome $o_i \in \{\pm 1\}$ and basis $b_i \in \{X, Y, Z\}$ are stored. The single-qubit Bloch vector estimator can be written as

$$\hat{r}_k = 3 \cdot \frac{1}{N_k} \sum_{i:b_i=k} o_i,$$

where $k \in \{X, Y, Z\}$ and N_k is the number of shots in basis k. The reconstructed state is then

$$\hat{\rho}_{\text{shadow}} = \frac{1}{2}(I + \hat{r}_x X + \hat{r}_y Y + \hat{r}_z Z).$$

2.3 Quantum State Tomography (QST)

QST performs separate measurement blocks for each basis. For basis $k \in \{X, Y, Z\}$:

1. prepare $|+\rangle$,
2. apply the appropriate basis rotation,
3. measure the outcome in the computational basis,
4. repeat this measurement 1000 times.

Total shots: 3000. Measurement outcomes $m_k \in \{0, 1\}$ are converted to Pauli expectation values via

$$\langle \sigma_k \rangle = 2\langle m_k \rangle - 1,$$

and the reconstructed density matrix is:

$$\rho_{\text{QST}} = \frac{1}{2}(I + r_x X + r_y Y + r_z Z).$$

2.4 Fidelity and Density Matrix Reconstruction

The fidelity with respect to $|+\rangle$ is computed as:

$$F = \langle + | \, \rho \, | + \rangle \, .$$

For a single qubit, the purity is given by:

$$\mathrm{Tr}(\rho^2) = \frac{1 + \|\vec{r}\|^2}{2},$$

where $\vec{r} = (r_x, r_y, r_z)$ is the Bloch vector.

All relevant quantities (Bloch vectors, density matrices, and fidelities) are computed for both QST and classical shadows from the recorded measurement data.

3 Results

3.1 Basis Sampling

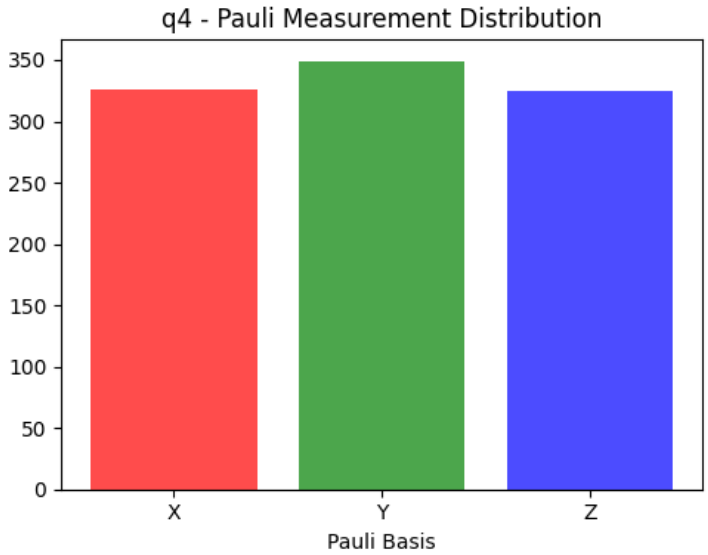

Figure 1: Histogram of Pauli basis sampling for classical shadows. The random selection produces nearly uniform sampling across X, Y, and Z.

Table 1 shows the number of times each Pauli basis was measured in the classical shadows experiment.

X	Y	Z
326	349	325

Table 1: Pauli basis sampling counts for classical shadows.

The sampling is close to uniform, as expected from random Pauli selection.

3.2 Reconstructed Bloch Vectors

Figure 2 shows the reconstructed Pauli expectation values for QST and classical shadows.

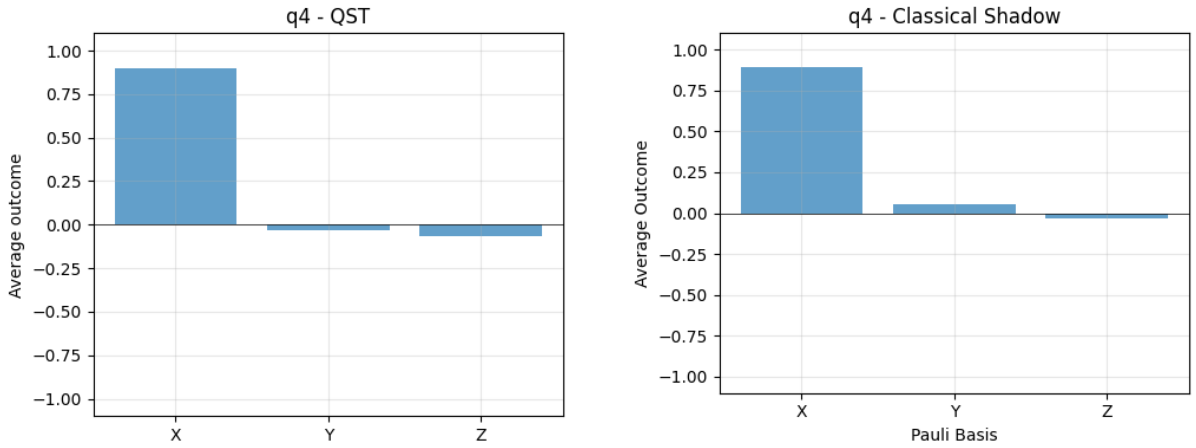

(a) QST reconstruction.

(b) Classical shadows estimate.

Figure 2: Comparison of QST and classical shadows Pauli expectation value reconstruction for qubit q4.

3.3 Bloch Sphere Visualization

We also visualize the reconstructed Bloch vectors from both methods on the Bloch sphere. Both vectors lie close to the ideal $+X$ direction, and the deviations in Y and Z components are small.

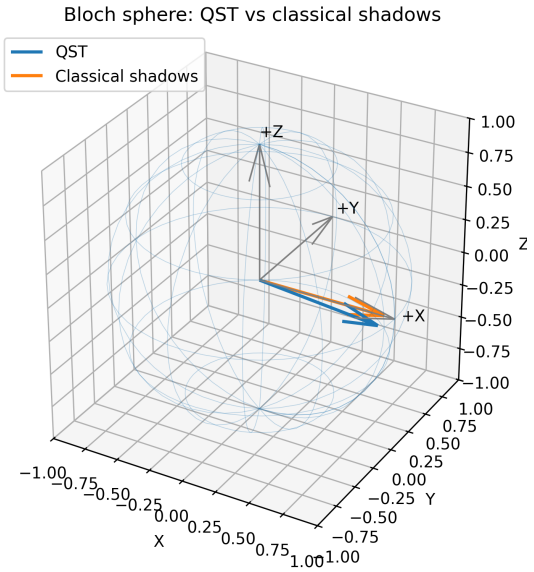

Figure 3: Bloch sphere showing the reconstructed Bloch vectors from QST and classical shadows. Both estimates lie near the ideal $|+\rangle$ state at the equator along the $+X$ axis.

The corresponding Bloch vectors from both QST and Classical Shadows are summarized in Table 2.

Method	r_x	r_y	r_z
QST	0.896	−0.030	−0.064
Classical Shadows	0.896	0.054	−0.034

Table 2: Estimated Bloch vectors for both methods.

Both methods reconstruct a state strongly polarized along $+X$, consistent with the target $|+\rangle$ state. The Y and Z components are small in magnitude in both cases, with classical shadows showing somewhat larger deviations due to its higher estimator variance per basis.

3.4 Density Matrices

From the Bloch vectors, we reconstruct the density matrices.

QST reconstruction:

$$\rho_{\text{QST}} = \begin{pmatrix} 0.468 & 0.448 + 0.015i \\ 0.448 - 0.015i & 0.532 \end{pmatrix}.$$

Classical shadows reconstruction:

$$\rho_{\text{shadow}} = \begin{pmatrix} 0.483 & 0.448 - 0.027i \\ 0.448 + 0.027i & 0.517 \end{pmatrix}.$$

Both reconstructions exhibit similar real off-diagonal coherence ($\text{Re}[\rho_{01}] \approx 0.448$), corresponding to the superposition in $|+\rangle$. The imaginary parts differ slightly, reflecting sampling noise and calibration imperfections, but remain small.

3.5 Fidelities

The fidelities with respect to the ideal $|+\rangle$ state for the latest runs are:

Method	Fidelity to $\|+\rangle$
QST	0.948
Classical Shadows	0.947

Table 3: Fidelity reconstruction comparison.

Remarkably, both methods yield essentially identical fidelities to three decimal places, confirming that classical shadows can match QST accuracy for this single-qubit task.

3.6 Runtime Comparison

The measured wall-clock execution times for both experiments were:

Method	Runtime (s)
QST	9.93
Classical Shadows	8.54

Table 4: Measured execution time of each method.

Classical shadows are modestly faster (by ~ 1.4 s), but both protocols complete within approximately 10 seconds. This indicates that the OPX controller overhead and fixed control-sequence execution time dominate over the incremental cost of additional measurement shots.

Method	Shots (total)	$F(\|+\rangle)$	r_x	Runtime (s)
QST	3000	0.948	0.896	9.93
Classical Shadows	1000	0.948	0.896	8.54

Table 5: Summary of shots, fidelity, main Bloch component, and runtime for QST and classical shadows.

4 Discussion

The experiment demonstrates that classical shadows and QST produce nearly identical reconstructions of the single-qubit $|+\rangle$ state. Both Bloch vectors and density matrices agree at the percent level, and the reconstructed fidelities are equal within our resolution ($F \approx 0.948$ for both methods). This confirms that classical shadows provide an efficient and unbiased estimator for single-qubit observables in this setting.

Although classical shadows use three times fewer structured measurement blocks (QST requires 1000 shots per basis, while shadows use 1000 shots in total), the observed runtime difference is modest. The classical shadows run is about 1.4 seconds faster, but both complete within roughly 10 seconds. This indicates that, in the single-qubit regime, hardware overhead (streaming, reset time, trigger latency, and control flow) dominates the total execution time, and the benefit of reducing the number of basis-specific shots is partially hidden.

In larger systems, classical shadows offer stronger theoretical advantages:

- QST requires 3^n measurement settings for n qubits.
- Classical shadows require only random single-qubit Pauli measurements.
- The number of shots needed grows primarily with the number of observables being predicted, rather than the full dimension of the Hilbert space.

Thus, while the present experiment shows near-parity between QST and shadows for a single qubit, it supports the expectation that classical shadows will become increasingly favorable as system size and observable count grow.

A natural next step is extending the experiment to two-qubit Bell states, where QST requires 9 distinct measurement settings but shadows can use the same random local Pauli sampling framework. Such an experiment would more clearly highlight the scaling benefits of classical shadows.

References

[1] Huang, H.-Y., Kueng, R., Preskill, J., "Predicting many properties of a quantum system from very few measurements," *Nature* 584, 2020.